Available online at www.sciencedirect.com
ScienceDirect
Cement & Concrete Composites 30 (2008) 138–151
Cement & Concrete Composites
www.elsevier.com/locate/cemconcomp

Prediction of compressive strength up to 28 days from microstructure of Portland cement

K. Svinning [a,*], A. Høskuldsson [b], H. Justnes [c]

[a] NORCEM A/S, Process and Environmental Department, Brevik, Norway
[b] Danish Technical University, Luntofte, Denmark
[c] SINTEF Building and Infrastructure, Concrete, Trondheim, Norway

Received 10 January 2007; accepted 30 May 2007
Available online 29 June 2007

Abstract

The influence of the characteristics or the microstructure of Portland cement on compressive strength up to 28 days has been statistically investigated by application of partial least square (PLS) analysis. The main groups of characteristics were mineralogy and superficial microstructure represented by curves from X-ray diffraction analysis and differential thermogravimetric analysis, as well as particle size distributions.

PLS gave maximum explained variance in compressive strength at 1, 2, 7 and 28 days of 93%, 90%, 79% and 67%, respectively. The high explained variance makes the prediction of the compressive strength up to 28 days from the characteristics reliable.

The prediction ability makes it possible in this case to predict strength from cement characteristics and vice versa. Such a prediction can be utilized to design a cement to achieve target strength performance.

Keywords: Compressive strength; Cement characteristics; Multivariate data analysis; PLS

1. Introduction

Since 1991 a general investigation of microstructure of clinker and cement has been carried out as part of several succeeding projects at the cement producer Norcem A/S. More recently, the investigations have been organised in the three following subprojects:

1. Influences of the production conditions in the kiln and the cement mill on the microstructure of clinker and cement.
2. Influences of the microstructure of clinker and cement on the cement properties.
3. Establishment of models describing the influences of the production conditions in the kiln and the cement mill on the cement properties.

Results from the previous investigations are published by Svinning et al. [1,2], Svinning and Bremseth [3] and Svinning and Justnes [4].

Cement chemists use the short hand notation $C = CaO$, $S = SiO_2$, $A = Al_2O_3$, $F = Fe_2O_3$, $\overline{S} = SO_3$, $N = Na_2O$, $K = K_2O$, $H = H_2O$, etc. According to this notation the main mineral in cement, Ca_3SiO_5, should be written C_3S for simplicity. Cement microstructure can be described as composite grains from ground clinker consisting of domains of crystalline alite (C_3S) and belite (C_2S) partly embedded in frozen melt phase (interstitials) from where they are grown while in the kiln. The interstitials consist basically of C_3A and C_4AF. These minerals can attain several crystalline modifications. Alite is usually in the monocline form due to lattice contaminations like magnesium and aluminium and rapid cooling. Alkalis like potassium and sodium are present in the clinker in the order of 0.5–1.0% Na_2O-equivalents and will end up as contaminants stabilising different crystal modifications of other

* Corresponding author. Tel.: +47 35572314; fax: +47 35570400.
E-mail address: ketil.svinning@norcem.no (K. Svinning).

0958-9465/$ - see front matter © 2007 Published by Elsevier Ltd.
doi:10.1016/j.cemconcomp.2007.05.016

compounds (e.g. potassium in β-C_2S or sodium in C_3A) or as sulphates like aphthitalite, $K_3N\overline{S}_4$. Gypsum is ground together with clinker to form cement with controlled setting time. However, the temperature in the mill can be so high that gypsum ($C\overline{S}H_2$) may dehydrate to hemihydrate ($C\overline{S}H_{1/2}$). The distribution of main minerals in a neat Portland cement (i.e. without any other mineral additions than calcium sulphate) may typically be of the order 60% C_3S, 20% C_2S, 10% C_4AF, 5% C_3A and 5% $C\overline{S}H_2$.

Out of a great number of papers or articles regarding predictions and explanation of variation in compressive strength development based on examination of microstructure only a small selection is introduced. The compressive strength at three days was predicted by Goswani et al. [5] to increase with increasing ratio between the pulse counts for belite and alite, respectively. The pulse counts mentioned in [5] were actually XRD-(X-ray diffraction) peaks at $d_1 \approx 2.78$ Å (*p.h.* 1) and $d_2 \approx 2.74$ Å (*p.h.* 2). Brüggemann and Brentrup [6] evaluated a formula which used the amount of soluble alkali and the amount and the mean chord length of alite for predicting strength of cement. A formula generated by Knöfel [7] for prediction of compressive strength at 28 days used the amounts of alite, belite, aluminates and ferrite as variables. The amounts of minerals included in the prediction models in [6,7] were determined by microscopy.

The results presented in [5] encouraged Svinning and Bremseth [3] to continue research on the influence of the microstructure on the cement properties by statistical investigations. Compressive strength up to 28 days was predicted to increase with an increase in (*p.h.*1/*p.h.*2). The other variables included in the investigation in [3] were the chemical composition from XRF (X-ray fluorescence), the amount of di- and hemihydrate of $CaSO_4$ and various mass losses upon heating (i.e. thermogravimetry) describing the degree of prehydration and carbonation of the clinker minerals and specific fineness. In the work by Svinning et al. [2] on XRD studies on variations in the microstructure of Portland clinker correlated with the variation in the production conditions in the kiln, the whole profiles of selected XRD-peaks were included in the investigation. Statistically, this could be carried out by applying multivariate rather than multivariable modelling.

A further step in evaluating a model of prediction from the microstructure of the cement was to include more complete characteristics of the cement in the form of profiles from XRD and TG (thermogravimetry), and a complete particle size distribution (32 size classes). A prediction model evaluated from partial least square regression (PLS) on 200 variables and 120 observations was presented in Svinning et al. [1]. The presentation of the regression coefficients was limited to those needed for the prediction of potential compressive strength of the clinker from the XRD-profile of the clinker part of the cement. Prediction of compressive strength from another part of the microstructure: particle size distribution of cement is presented in Svinning [8]. In this work, more observations have been added to the observation **X**-matrix for inclusion in the PLS.

Beside ordinary multivariable regression, fuzzy logic [9], stepwise regression [10], genetics algorithms-artificial neural networks (GAs-ANNs) [11] and PLS [1–4,8] have been applied in the evaluation of the model for prediction of cement strength. GAs-ANNs and PLS represent different types of multivariate calibration or modelling with hidden layer or latent variables. In [8] the latent variables were taken into consideration in the sensitivity analysis, while in [11] the hidden layers were not. [8] shows examples of sensitivity analysis in the form of simulated variation of a latent variable from which cement properties are predicted.

The objective of this work was to establish a statistical model for the prediction of cement properties for all types of neat cement as well as cement containing small amounts (~5%) of limestone filler. To attain this objective, variables which presented a complete characterisation of the microstructure of the cement, and observations which represented a great variety of types of cement, were included in the PLS.

2. Methods

2.1. Characterisation of the microstructure of clinker

The XRD analysis was performed on ground clinker. The XRD-profiles consisted of intensities at every 0.02°. The scaling of the intensities and adjustment of the 2θ-position of the diffraction peaks were based on normalisation of the area and adjusting the 2θ-axis to match the diffraction peak at $d = 3.52$ Å for anatase (TiO_2), which was intermixed in an amount of 10 wt% of the total sample. Examples of diffractograms including the peak of the reference are shown in Fig. 1. To reduce the number of intensities (and the number of variables) and simultaneously increase the signal to noise ratio one variable was made out of three by averaging three adjacent variables in the diffraction profile before including the variables in PLS. The number of variables was further decreased by selecting two small regions (2θ) of diffractogram 29.88–30.70° and 32.90–34.10° (using CuKα-radiation) to be included in the modelling.

2.2. Characterisation of superficial microstructure

As mentioned above, the superficial microstructure is characterised by thermogravimetry (TG) analysis. The TG apparatus applied was a Netzsch STA – Apparatur 409 V/3/C®. A dynamic mode of thermogravimetry is used, in which the sample is heated in an environment whose temperature is changing in a predetermined manner, preferably at a linear rate. Weights of samples analysed were 4.2 g and the heating rate was 2 K/min. Fig. 2 shows two examples of thermograms from DTGA of neat cement and cement with limestone used as filler, respectively. The

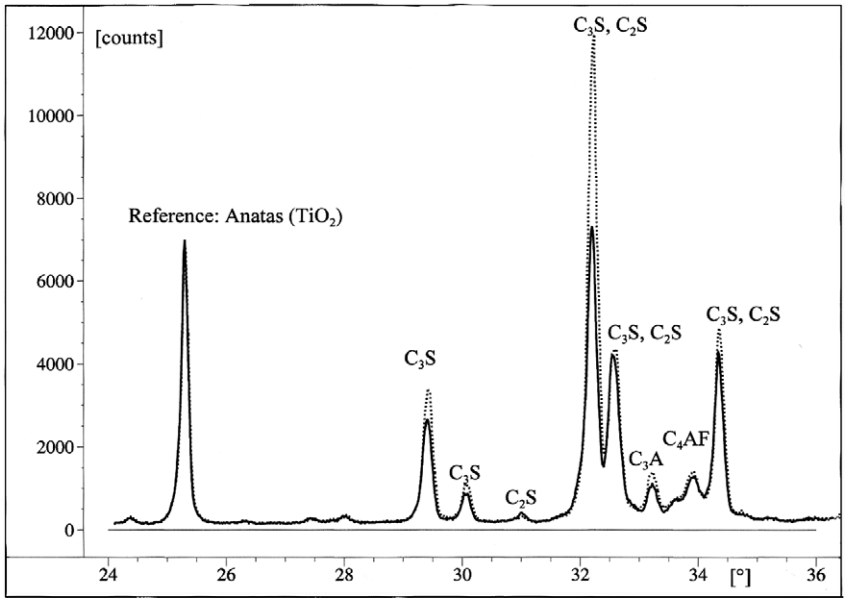

Fig. 1. Examples of two X-ray diffractograms of two neat cements in the 2θ range 24–36°.

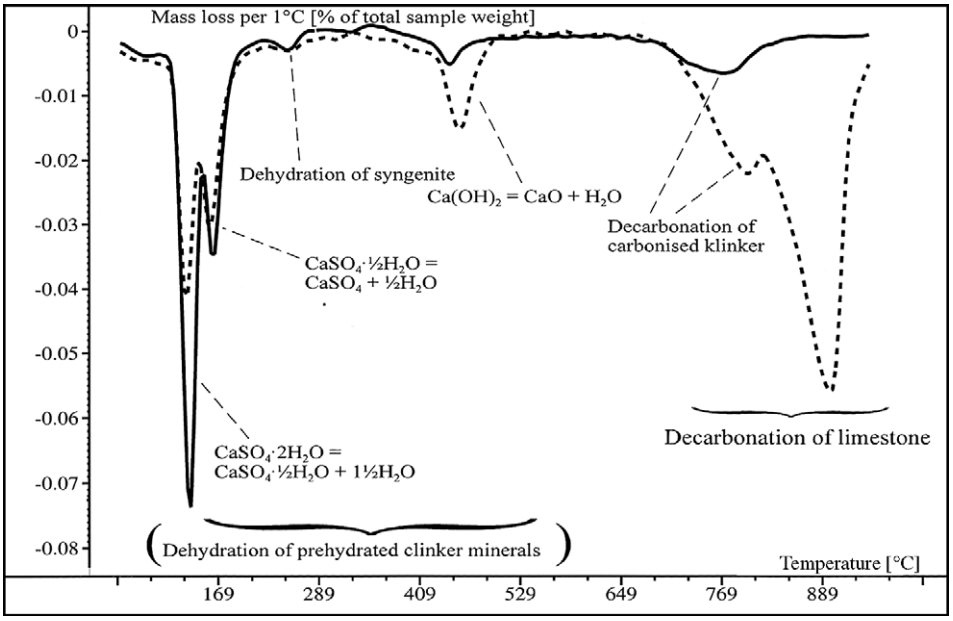

Fig. 2. Two examples of DTG (differentiated thermogravimetry) curves for neat cement and cement with limestone filler, respectively.

thermograms are interpreted with respect to the most common reactions occurring during the heating.

The information about superficial microstructure is included as x- or y-variables in PLS in the form of mass loss per 4 °C in the temperature range 20–330 °C and mass loss per 8 °C in the range 330–940 °C. No further interpretation of the results from DTGA prior to PLS was done.

2.3. Statistical modelling

In the case of a large number of variables relative to the number of observations or objects, data compression by expressing the original x-variables by fewer latent variables or factors could be necessary. Partial least square regression (PLS) does calculation and optimisation of a number of factors for maximum explanation of variance in the y-variables. In addition, model parameters are calculated for prediction of y for new values of the x-variables. In this work, PLS was performed on several y-variables combined expressed as a vector. The models which relate the PLS-model terms are then given by the two expressions in the equations below:

$$\mathbf{X} = \mathbf{T}\mathbf{P}^T + \mathbf{E} \tag{1}$$

$$\mathbf{Y} = \mathbf{U}\mathbf{Q}^T + \mathbf{F} \tag{2}$$

T and **U** are factor scores, **P** and **Q** are x and y-variables loadings and **E** and **F** are the residuals in **X** and **Y**, respectively. Alternatively, Eq. (1) could be expressed in the form:

$$\mathbf{X} = \mathbf{t}_1\mathbf{p}_1^T + \mathbf{t}_2\mathbf{p}_2^T + \cdots + t_k\mathbf{p}_k^T + \cdots + \mathbf{t}_l\mathbf{p}_l^T + \mathbf{E} \tag{3}$$

l is equal to maximum number of latent variables for maximum explanation of variance in **Y**. If there is only one y-variable to be modelled Eq. (2) could be replaced by the following equation:

$$\mathbf{y} = \mathbf{T}\mathbf{q}^T + \mathbf{f} \tag{4}$$

PLS with one or several y-variables is denoted PLS1 or PLS2, respectively. In case of PLS1 the regression coefficients to be used in the predictor $\hat{\mathbf{y}} = \mathbf{1}b_0 + \mathbf{X}\hat{\mathbf{b}}$ are computed as follows:

$$\hat{\mathbf{b}} = \widehat{\mathbf{W}}(\widehat{\mathbf{P}}^T\mathbf{W})^{-1}\hat{\mathbf{q}} \tag{5}$$

$$\text{and} \quad b_0 = \bar{y} - \bar{\mathbf{x}}^T\hat{\mathbf{b}} \tag{6}$$

where **W** are loading weights used in PLS1.

Similarly, for PLS2:

$$\widehat{\mathbf{B}} = \widehat{\mathbf{W}}(\widehat{\mathbf{P}}^T\widehat{\mathbf{W}})^{-1}\widehat{\mathbf{Q}}^T \tag{7}$$

and $\mathbf{b}_0^T = \bar{\mathbf{y}}^T - \bar{\mathbf{x}}^T\widehat{\mathbf{B}}$

By scaling the variables, unreasonable domination of variables with dominating standard deviations, $s(x)$, on the model can be avoided. The weighting of $x_{i,k}$ by centring and scaling is performed according to the following formula:

$$x_{ik,w} = \frac{x_{ik} - \bar{x}_k}{s(x_k)} \tag{8}$$

The type of validation applied in this work is cross validation. Validation means to determine the number of PLS-components or latent variables that give the prediction of y from **X** in future objects that lack the value of the y-variable. In this work, the calibration set was split into 10 segments, and the validation was repeated 10 times, each time treating one-tenth of the calibration set as prediction objects. The cross validated residual variance in y after inclusion of n latent variables is as follows:

$$\mathrm{Var}(y)_{\mathrm{val},n} = \frac{1}{I_{\mathrm{pr}}}\sum_{i=1}^{I_{\mathrm{pr}}}(\hat{y}_i - y_i)^2 \tag{9}$$

where I_{pr} is equal to the number of validation objects, which is equal to the number of the calibration objects. $\hat{y}_i$ is the predicted value and y_i the respective observed value. The explained variance of the total variance in y, $\mathrm{Var}(y)_0$, is calculated in this way

$$\mathrm{Expl.Var.}(\%) = \frac{\mathrm{Var}(y)_0 - \mathrm{Var}(y)_{\mathrm{val},n}}{\mathrm{Var}(y)_0} \tag{10}$$

Other quality criteria, which describe the validity of the prediction, are the root mean square error of prediction (RMSEP), the bias and the standard error of prediction. The parameters are calculated by the following formulas:

$$\mathrm{RMSEP} = \sqrt{\mathrm{Var}(y)_{\mathrm{val},n}} \tag{11}$$

$$\mathrm{Bias} = \frac{1}{I_{\mathrm{pr}}}\sum_{i=1}^{I_{\mathrm{pr}}}(\hat{y}_i - y_i) \tag{12}$$

$$\mathrm{SEP}^2 \approx \mathrm{RMSEP}^2 - \mathrm{Bias}^2 \tag{13}$$

The iterative algorithms for calibration, validation and prediction are described in detail in Martens and Næs [12]. The software applied for PLS was UNSCRAMBLER®, version 7.5.

3. Experimental

The types of cement included in the investigation, with reference to European (EN) and in addition, Norwegian Standards (NS) where they differ by national addendum, are as follows:

1. Low alkali, sulphate resistant cement, EN 197-1-CEM I 42.5 R, NS 3086-CEM I R-SR-LA.
2. Low alkali, high strength cement, EN 197-1-CEM I 52.5 N, NS 3086-CEM I 52.5 N-LA.
3. Standard Portland cement, EN 197-1-CEM I 42.5 R.
4. Rapid Portland cement, EN 197-1-CEM I 42.5 R, NS 3086-CEM I 42.5 RR.

Table 1 contains the typical mineral composition (calculated from the chemical composition by Bogue's formula) in the clinker used in the different types of cement presented above.

Some of the samples of Standard Portland cement, EN 197-1-CEM I 42.5 R, contained limestone filler.

Table 1

Mineral and chemical composition (%)	Sulphate resistant	High strength	Standard Portland	Rapid Portland
C_2S	16	12	13	12
C_3S	60	66	62	66
C_3A	0.5	6.1	7.7	6.1
C_4AF	15.8	11.0	10.0	11.0
Free lime	0.8	1.1	1.3	1.4
Na_2O-equiv.	0.53	0.55	1.05	1.15

Table 2
Results from PLS2 of compressive strengths up to 28 days as functions of the characteristics of the cement

Response variable, y	Maximum explained variance (%) with eight PLS-components included
Total	82
Compressive strength at one day	93
2 days	90
7 days	79
28 days	67

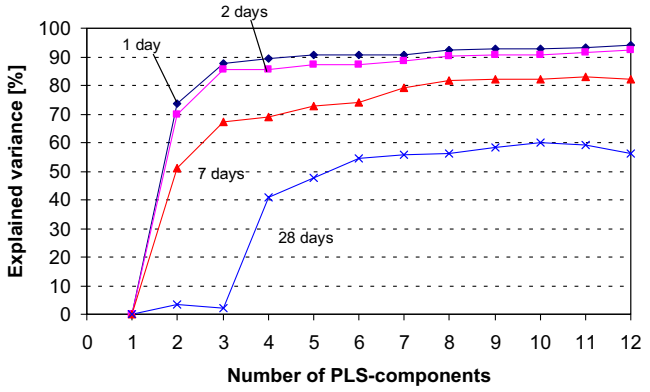

Fig. 3. Explained variances in compressive strength at 1, 2, 7 and 28 days versus the number PLS-component included in PLS2.

The *y*-variables: Compressive strengths at 1, 2, 7 and 28 days, were measured according to EN 196-10. The observation **X**-matrix consisted of 146 observations and 205 variables. The *x*-variable could be divided into the following groups or categories:

1. Mineralogy of the clinker part of the cement described by X-ray diffractogram sequences were taken as variables no. 1–14, 17–37.
2. Variables no. 38–106 and 137–213 were the superficial microstructure of the cement as described by thermograms from DTGA.
3. Particle size distribution of the cement were taken into account by variables no. 110–136.
4. Variables no. 15 and 16 consisted of the amount of SO_3 and free lime.

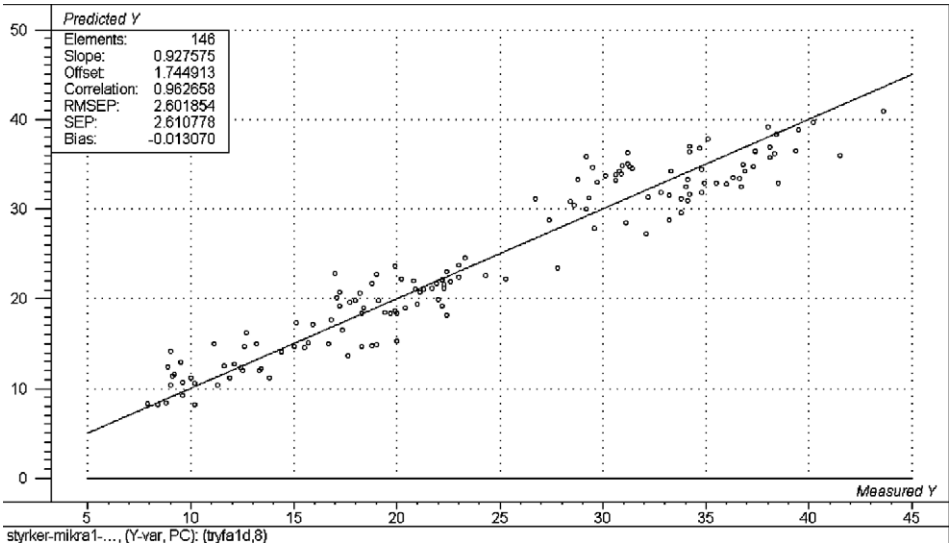

Fig. 4. Predicted versus measured compressive strength (MPa) at one day.

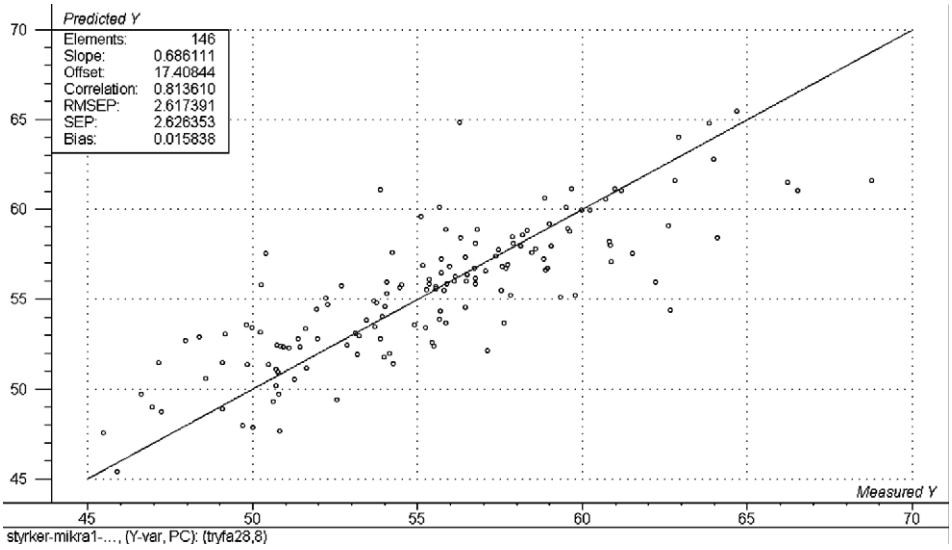

Fig. 5. Predicted versus measured compressive strength (MPa) at 28 days.

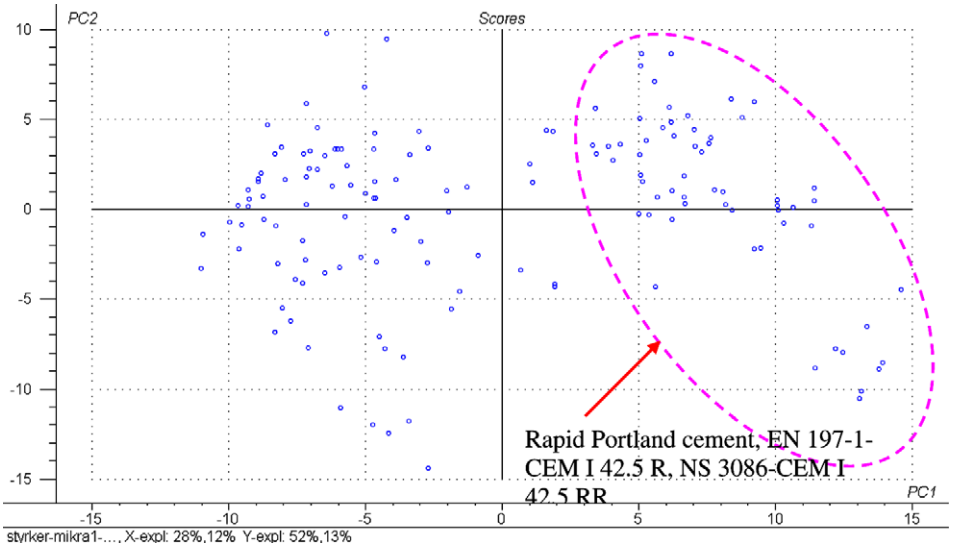

Fig. 6. 2-vector score plot for objects included in PLS. Levels of PLS-component no. 1 (PC1) and 2 (PC2) in each object.

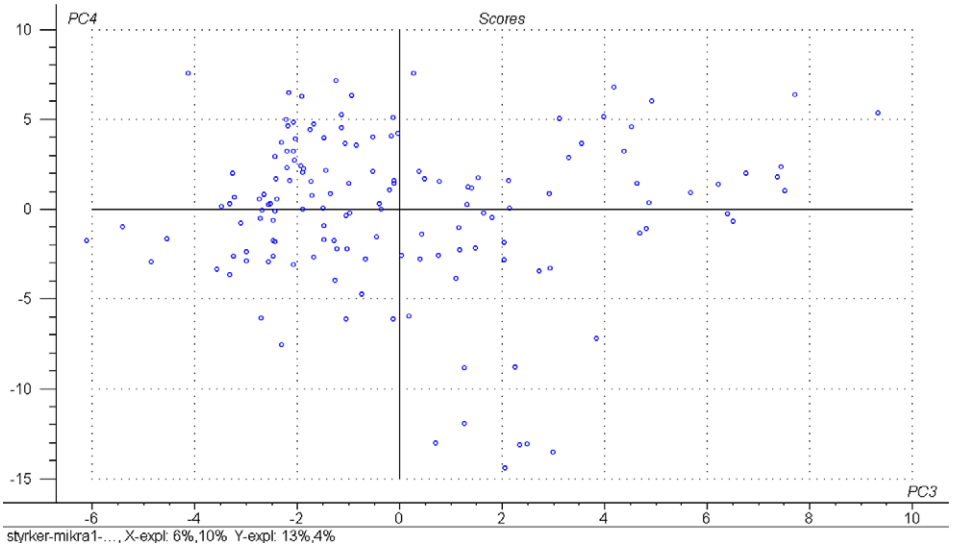

Fig. 7. 2-vector score plot for objects included in PLS. Levels of PLS-component no. 3 (PC3) and 4 (PC4) in each objects.

4. Results and discussion

The maximum explained variance from PLS of the respective *y*-variables and the number of PLS-components included for maximum explanation are presented in Table 2. Fig. 3 shows[1] the explained variance in compressive strength up to 28 days versus number of PLS-component or latent variables included. Predicted versus measured compressive strengths at 1 and 28 days are plotted in Figs. 4 and 5, respectively.

Fig. 4 demonstrates that the predicted versus measured compressive strength at 1 day fits the target line (predicted equal to measured) better than what is the case for compressive strength at 28 days in Fig. 5. This coincides with explained variances in the two properties from PLS. However, the points in Fig. 4 are not evenly distributed along the target line as in Fig. 5. This is confirmed by a group in the 2-vector score plot (PLS-component no. 1 and 2) shown in Fig. 6. The distinct group marked in Fig. 6 represents samples of cement of the type EN 197-1-CEM I 42.5 R, NS 3086-CEM I 42.5 RR. The relevant 2-vector score plot to find groups that have an influence on the prediction of compressive strength at 28 days is depicted in Fig. 7, which shows levels of PLS-component no. 3 and 4 in each objects. No distinct groups similar to the one in Fig. 6 can

[1] For interpretation of colors in Figs. 3, 6, 7 and 15–17, the reader is referred to the web version of this article.

be seen. Score plots could reveal if there are any outliers, i.e. observations that deviate statistically from the others, appearing as scores located relatively far away from the others. Working further with the data from [1] some of the outliers were removed before a new PLS.

According to the information in Fig. 3 the two first latent variables contribute very little to the explanation of variance in compressive strength at 28 days compared to compressive strength at an earlier age. From this observation, a separate PLS-model for prediction of strength at 28 days could be evaluated. 2-vector loading plots, examples of which are shown in Figs. 8 and 9, the figures not only show which of the variables are the most important for each PLS-component but also show correlation between the different variables. The figures contain correlation loadings, i.e. loadings marking 50% and 100% explained variance limits. Correlation loadings are helpful in revealing variable correlation. The loading plot in Fig. 8 confirms the low explained variance in compressive strength at 28 days including only PLS-component no. 1 and 2 while the explained variance in compressive strength up to 7 days is more than 50%. The loading plot shows also a positive correlation between the early strengths and one part of the variables describing the particle size distribution, located very close to each other. Simultaneously, the early strengths are negatively correlated to another part whose variables are lying along the diagonal through the *y*-variable and origin equidistantly on the other side of

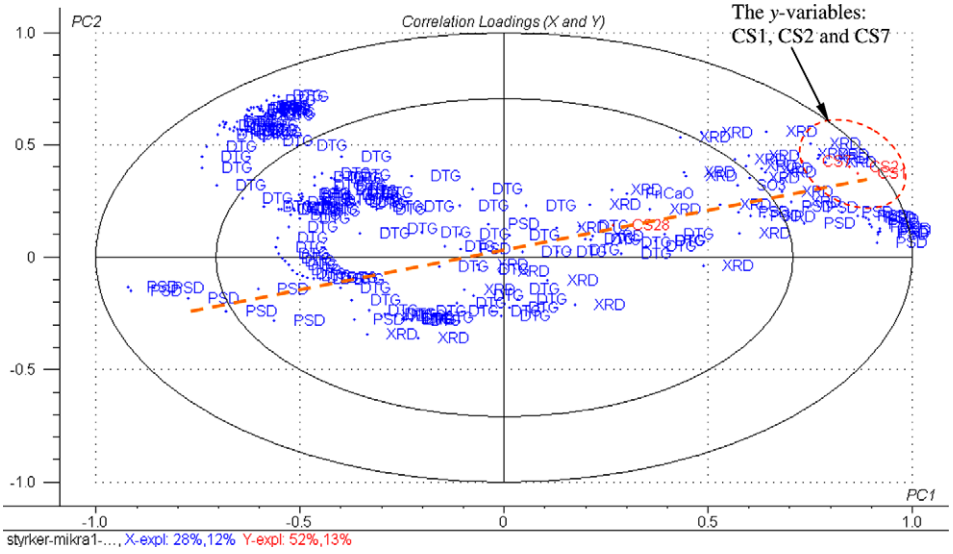

Fig. 8. 2-vector plot, *x*- and *y*-loadings for PLS-component no. 1 (PC1) and no. 2 (PC2). The variable legend refers to the analysis giving the value of variables: XRD = X-ray diffraction, DTG = differential thermogravimetry, PSD = particle size distribution and CS1, CS2, CS7 and CS28 = compressive strength at 1, 2, 7, and 28 days, respectively.

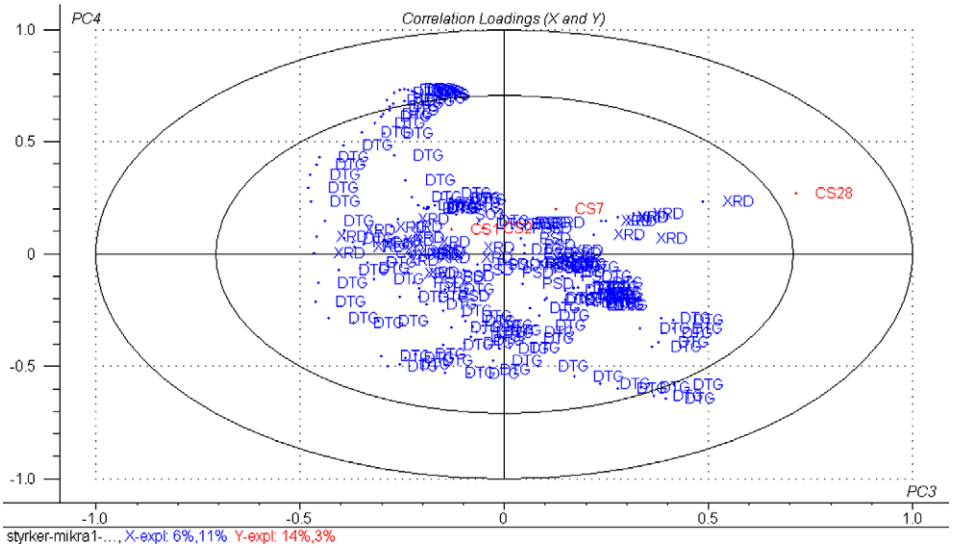

Fig. 9. 2-vector plot, *x*- and *y*-loadings for PLS-component no. 3 (PC3) and no. 4 (PC4). The variables presented here are the same as in Fig. 8.

origin. As expected, compressive strength at early ages correlates strongly with the fineness and the particle size distribution (PSD) of cement. The loading plot in Fig. 8 reveals that early strength also correlated with variables (labelled XRD) describing mineral composition and structure, while compressive strength according to Fig. 9 correlates more with the XRD- than the PSD-variables.

Figs. 10–14 show (a) the variation of and (b) the regression coefficient, $\mathbf{b}_w$, for prediction of compressive strengths up to 28 days from the variables presented in the experimental section. The regression coefficients $\mathbf{b}_w$: $b_{w1}, b_{w2}, \ldots, b_{wK}$ used in the prediction model $y_w = b_{0w} + b_{w1}x_{1,w} + b_{w2}x_{2,w} + \cdots + b_{wK}x_{K,w}$ for prediction of the four y-variables in centred and scaled form are presented in Figs. 10–14. The elements in $\mathbf{b}_w$, contrary to the respective elements in $\mathbf{b}$ used for prediction from the x-variables in their original forms, i.e. neither centred nor scaled, give the information about how much each x-variable influences the y-variables. Looking at 10b, $\mathbf{b}_w$ for predicting compressive strength at 28 days indicate that the compressive strength at 28 days will decrease with increasing amount of aphthitalite having a peak at $2\theta = 30.38°$ and increase with a shift of the C_3S-peak from $2\theta = 30.09°$ to $2\theta = 30.04°$.

However, $\mathbf{b}_w$ defined as an indicator of influence could be somewhat misleading, if the confidence intervals of $\mathbf{b}_w$ are not taken into consideration. Martens and Martens [13] have developed an improved method for uncertainty testing based on cross validation, Jack knifing, and stability plot. To obtain a better interpretation of $\mathbf{b}_w$, the standard deviations of the respective variables should be presented too. Alternatively, picking out every fifth observation of the variation, as illustrated in Figs. 10–14a, will give an idea about variance. However, $\mathbf{b}$ cannot then be calculated directly from $\mathbf{b}_w$.

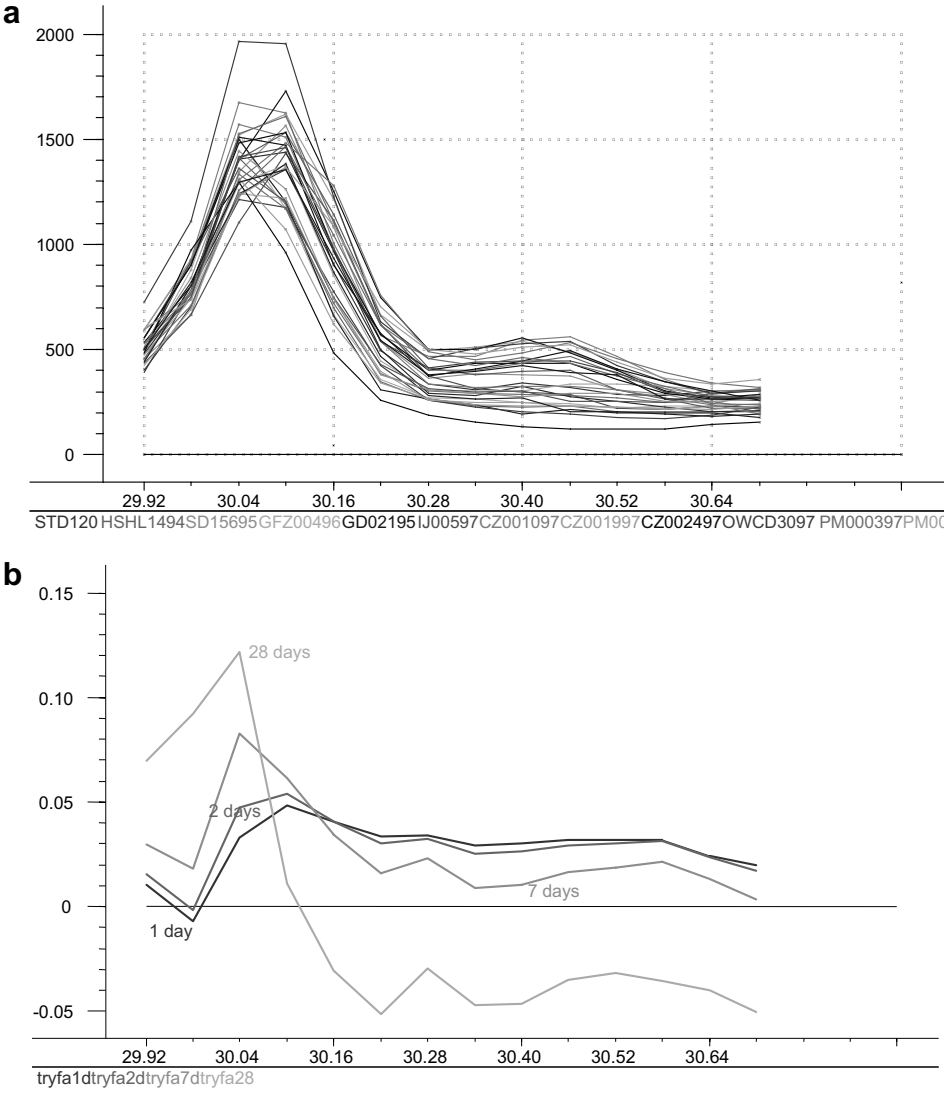

Fig. 10. Results from PLS for prediction of compressive strength at 1, 2, 7 and 28 days from XRD intensities in the 2θ-region 29.92–30.70° (abscissa). (a) Variation in the variables no. 1–14 (ordinate has unit XRD counts). (b) The respective regression coefficients, $\mathbf{b}_w$, for prediction of compressive strengths as ordinate.

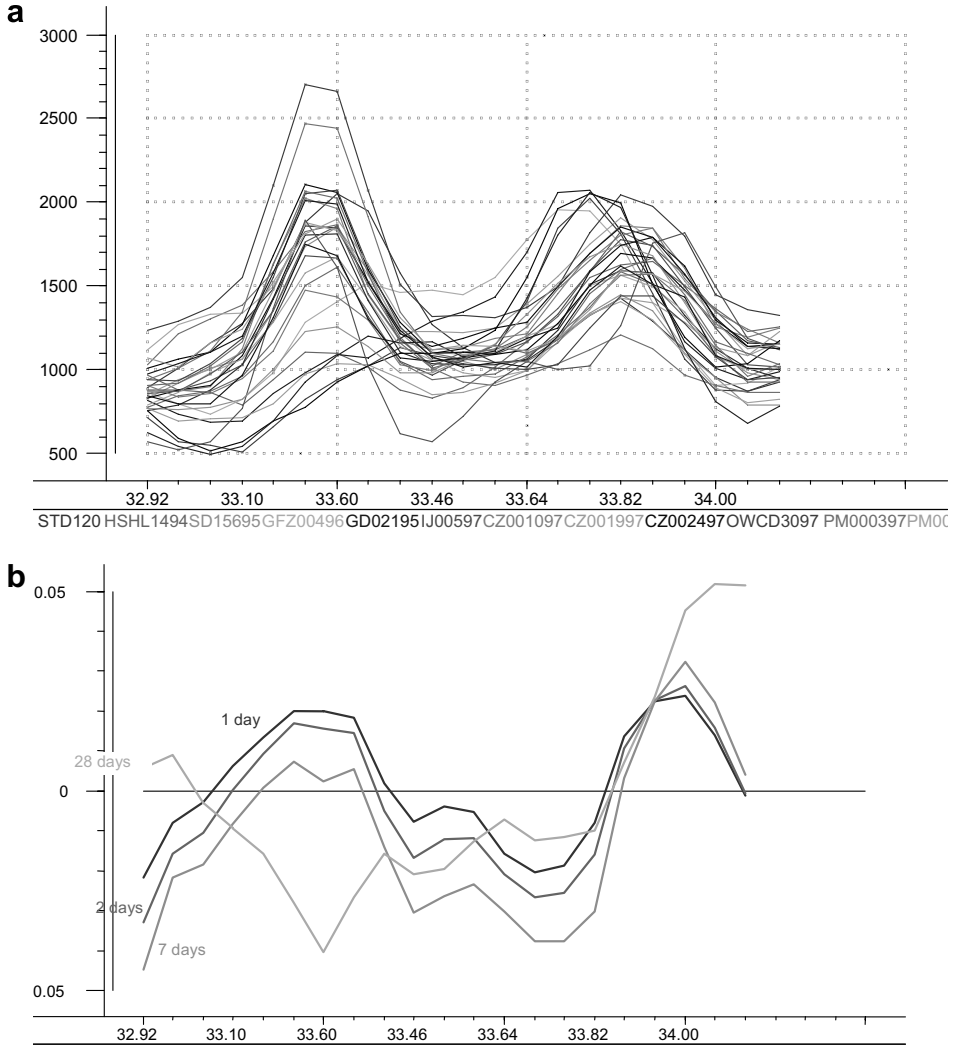

Fig. 11. Results from PLS for prediction of compressive strength at 1, 2, 7 and 28 days from XRD intensities in the 2θ-region 32.92–34.10° (abscissa). (a) Variation in the variables no. 17–37 (ordinate has unit XRD counts). (b) The respective regression coefficients, $\mathbf{b}_w$, for prediction of compressive strengths as ordinate.

The mineral composition could be determined by multi-component Rietveld analyses. Instead of including selected parts of the diffractogram, which requires a lot of variables to describe the profiles, only a few variables giving the whole mineral composition would need to be included in PLS. However, the inaccuracy of the amount of a mineral determined by Rietveld analyses will increase with decreasing amount of the mineral. C_3A could also exist as two polymorphs, cubic and orthorhombic, with different reactivity. Having a total amount of C_3A, as calculated by the Bogue methodology, like for instance 5%, split into polymorphs could lead to fairly high inaccuracy in calculation of the amount of each. The benefits of including the XRD-profile as it has been done here are that (a) no information would be lost, and (b) any change in structure or unit cell dimensions due to foreign ion contamination or interchange would be detected directly by changes in the position of the respective peaks. Such structural changes of the minerals may influence their reactivity towards water leading to changes in properties like compressive strength up to 28 days as shown by Svinning et al. [1]. The minerals giving rise to reflections in the two selected diffraction angle ranges are listed in Tables 3 and 4.

As seen from Table 3, the range $2\theta = 29.88$–$30.70°$ contains information solely on alite and aphthitalite, $K_3Na(SO_4)_2$ (i.e. other known cement minerals have no reflections in this region). Although the intensities of the two overlapping alite reflections are modest, the domination of this mineral in Portland cement secures a good signal to noise ratio for this mineral. Alite is dominating the early strength development, as is well known. One of the strongest reflections of aphthitalite is in the high end of this first XRD region, and it can give valuable information on this easily soluble alkali sulphate. In spite of its low content, aphthitalite can dominate the early pore water chemistry and strongly influence for instance setting time. Note that calcite interground in some cements has its strongest reflection at 29.4°. This means that the tail of the main

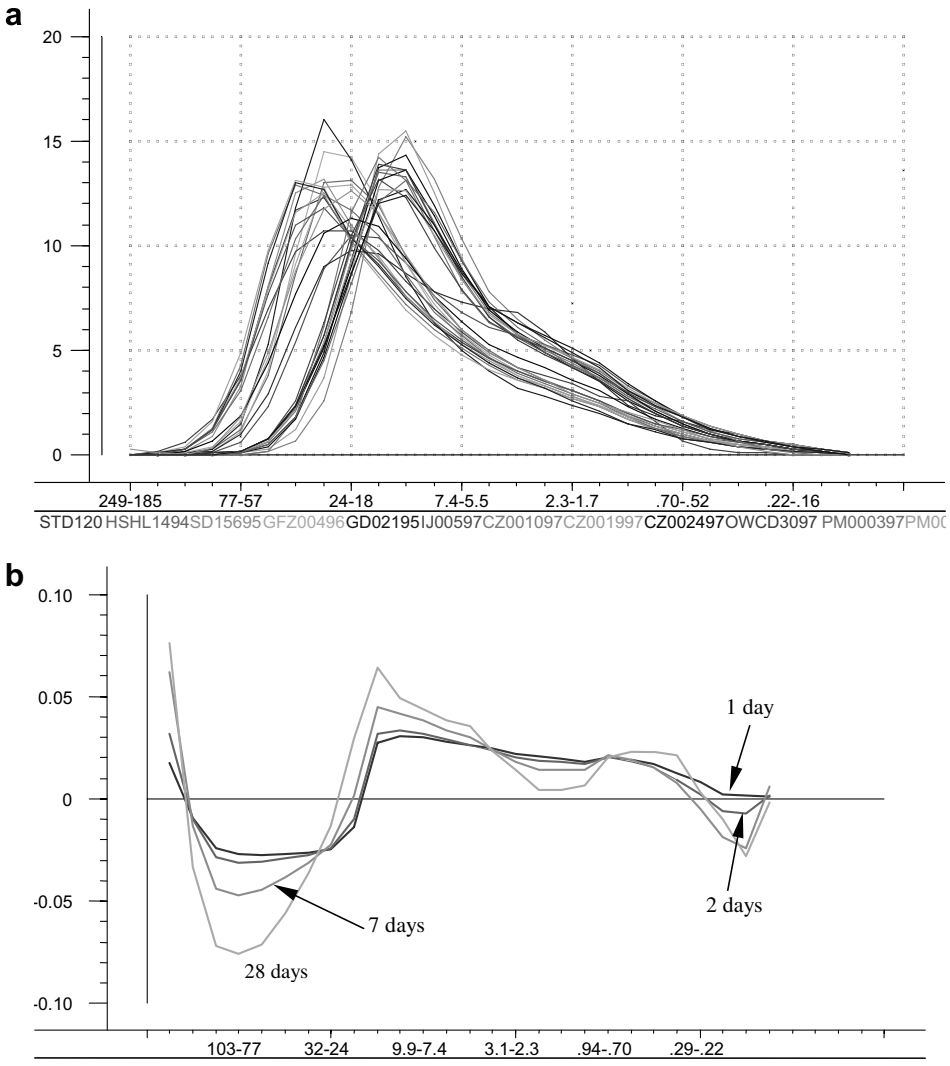

Fig. 12. Results from PLS for prediction of compressive strength at 1, 2, 7 and 28 days from volume fractions of cement in 27 size classes between 249 and 0.09 μm (abscissa). (a) Variation in the variables no. 110–136 (ordinate is volume fraction). (b) The respective regression coefficients, $\mathbf{b}_w$, for prediction of compressive strengths as ordinate.

calcite peak may reach into the 29.88–30.70 2θ range. Table 4 lists the only cement minerals contributing to the reflections in the range $2\theta = 32.90$–$34.10°$. This second XRD region is not only dominated by reflections of C_3A and C_4AF, but it also contains the dominating reflection of the more seldom clinker minerals α'-C_2S and mayenite, $C_{12}A_7$. The common clinker phase belite, β-C_2S, also has a modest reflection in the low end of this region. However, since alite and belite are the only silicate phases, an increase in alite content will lead to a decrease in belite content, so an independent control of the latter is not required. For cement analysis, it is also of interest that gypsum has a medium reflection in the high end of this second XRD region. Thus, the two selected XRD regions cover the responses for all the important cement minerals, and are a more direct measure of the actual content of each mineral since the simple Bogue calculation (see Table 2) at best is an indication of the cement composition.

According to general experiences, the superficial microstructure should influence compressive strength at one day more than the strength at 28 days. $\mathbf{b}_w$ shown in Fig. 13b and Fig. 14b could indicate the opposite. $\mathbf{b}_w$ for predicting compressive strength at 28 days from some of the variables is surprisingly high taking into account the variations of the variables depicted in Fig. 13a and Fig. 14a. To examine the significance of the influence of **x** on **y,** uncertainty testing on $\mathbf{b}_w$ giving confidence interval of each $\mathbf{b}_w$ was performed. Figs. 15 and 16 show $\mathbf{b}_w$ inclusive confidence interval of 95% for prediction of compressive strength at 1 and 28 days, respectively, from the variables presented in Fig. 14a. Evaluation of the significance of the influence of a variable x_k from Jack knifing estimation could be defined significant if the uncertainty level is less than $2|\mathbf{b}_{wk}|$. From this criterion, the influence of the actual variables on the compressive strength at 28 days can be considered to be less significant than the analogues influence on compressive

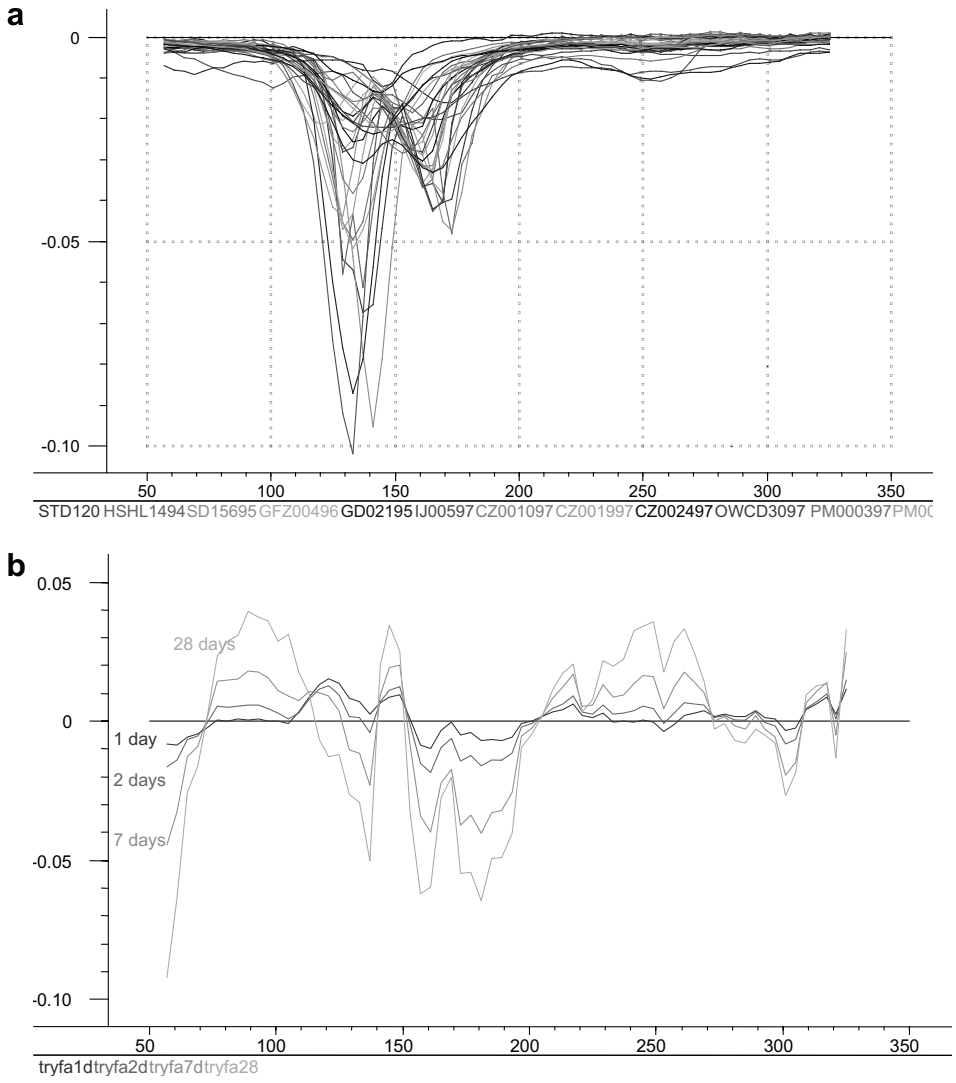

Fig. 13. Results from PLS for prediction of compressive strength at 1, 2, 7 and 28 days from mass loss per 4 °C from DTG in the temperature range 57–325 °C (abscissa). (a) Variation in the variables no. 38–106 (DTG values are ordinate). (b) The respective regression coefficients, $\mathbf{b}_w$, for prediction of compressive strengths as ordinate.

strength at one day. The same consideration can be made for the variables presented in Fig. 13. In general, the variables describing the superficial microstructure can be considered to influence the compressive strength at 28 days less than the compressive strength at one day.

Examples of influence of the structure of minerals on the strength development, as well as influence of the amount the minerals, can be discovered comparing Fig. 10a and b and Fig. 11a and b, respectively. The variation of the position of the XRD-peak of C_3S shown in Fig. 10b indicates variations in the contaminants of C_3S (i.e. the structure is the same, but the unit cell axes may vary). The form and threshold of the curves of $\mathbf{b}_w$ indicate that the structure of C_3S has an great impact on compressive strength at both 1 and 28 days. A C_3S-peak at $2\theta < 30.04°$ will give a low compressive strength at one day and high strength at 28 days. For C_3S having an XRD-peak at $2\theta > 30.04°$ the opposite will be the result. However, note that since limestone has its strongest peak at 29.4°, the tail of this peak for cements with 4% interground filler may make it appear as the C_3S-peak has shifted to a lower value. By comparing Fig. 11a and b a variation in the structure of C_3A is indicated giving variation mostly in compressive strength at one day. The variation in the structure of C_3A is according to Taylor [14] a shift from orthorhombic to cubic structure due to a decrease in amount of sodium. The variation in the structure of C_3S is more difficult to explain (may be due to limestone influence).

Instead of including spectral variables as those describing XRD- and DTGA-curves, fewer variables presenting the interpretation of the curves could be included. A classical example of interpretation is determination of the amount of di- and hemihydrate of $CaSO_4$ from differential scanning calorimetry (DSC) analysis. A successful determination is conditional on having well separated peaks describing the dehydration of $CaSO_4 \cdot 2H_2O$ in two steps.

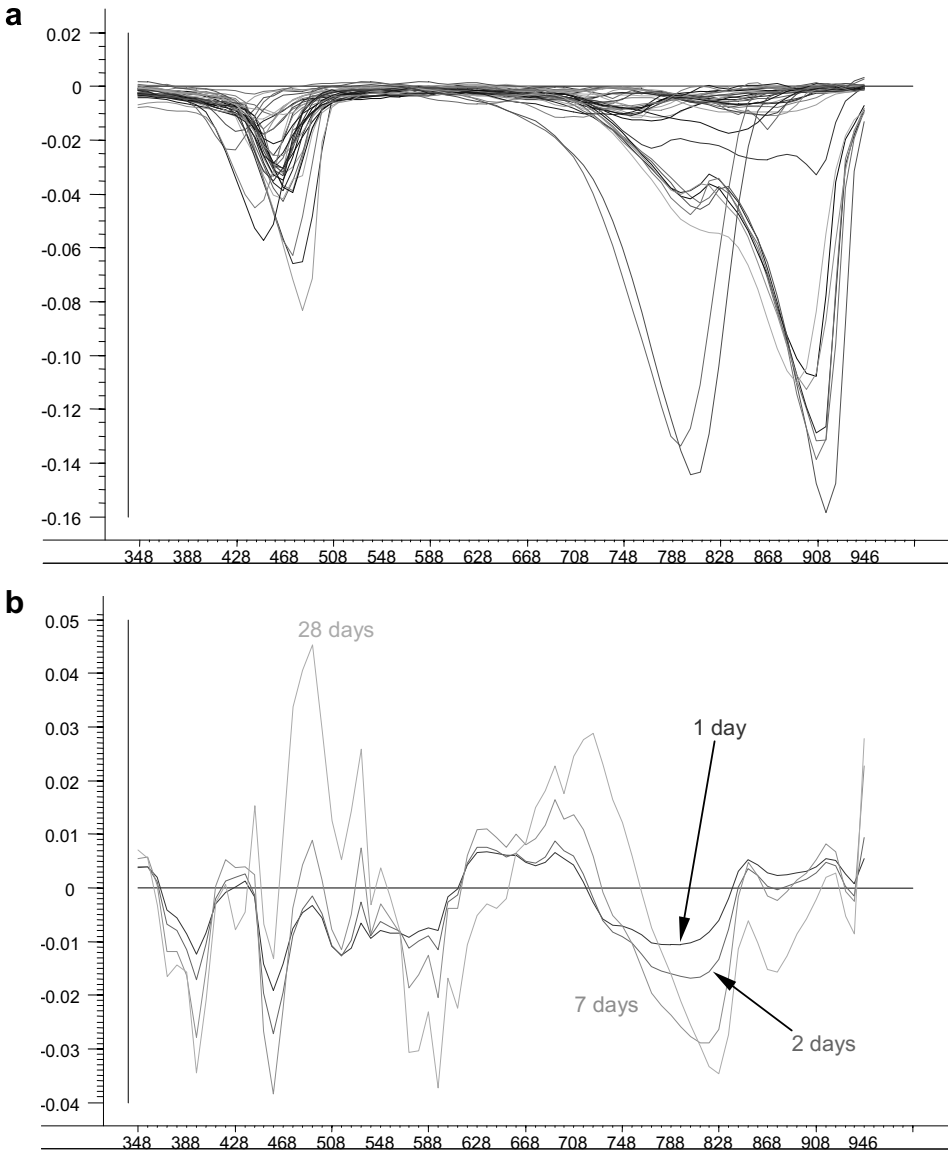

Fig. 14. Results from PLS for prediction of compressive strength at 1, 2, 7 and 28 days from mass loss per 8 °C from DTGA in the temperature range 348–950 °C (abscissa). (a) Variation in the variables no. 137–213 (DTG values are ordinate). (b) The respective regression coefficients, $\mathbf{b}_w$, for prediction of compressive strength as ordinate.

Table 3
Major phases within the XRD range $2\theta = 29.88$–$30.70°$

Phase	2θ (°)	d (nm)	Indices $\langle hkl \rangle$	Intensity (rel)
Alite (M3)	30.04	0.2975	⟨804⟩	10
	30.09	0.2970	⟨620⟩	20
Aphthitalite	30.38	0.2940	⟨102⟩	75

Table 4
Major phases within the range $2\theta = 32.90$–$34.10°$

Phase	2θ (°)	d (nm)	Indices $\langle hkl \rangle$	Intensity (rel)
Belite, β-C_2S	32.98	0.2716	⟨121⟩	38
α′-C_2S	33.65	0.2663	⟨260⟩	100
Cubic C_3A	33.26	0.2694	⟨044⟩	100
Orthorhombic C_3A	33.27	0.2693	⟨224⟩	100
	33.04	0.2711	⟨040⟩	25
	32.93	0.2720	⟨400⟩	31
$C_{12}A_7$	33.41	0.2680	⟨420⟩	100
C_4AF	33.84	0.2649	⟨141⟩	100
	33.64	0.2664	⟨002⟩	47
Gypsum	33.35	0.2684	⟨150⟩ and ⟨220⟩	50

Achievement of such a separation requires less amount of sample and a smaller crucible + lid with an aperture so small that it allows only diffusion controlled transport of vapour of water out of the crucible. In our case the similar two peaks from DTGA are not quite separated. The determination of di- and hemihydrate will be too inaccurate. Instead, the variables describing the DTGA-curves should therefore be included. Nevertheless, a qualitative interpretation of the curves could be useful to explain the

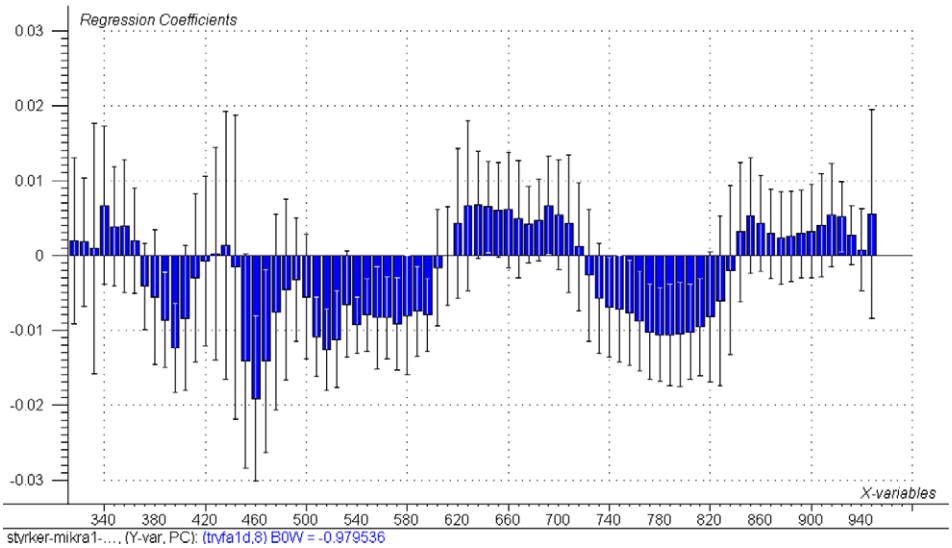

Fig. 15. Results from uncertainty testing on the regression coefficient, $\mathbf{b}_w$ (ordinate), for prediction of compressive strength at one day from the variables presented in Fig. 14 giving confidence intervals of 95%. Abscissa indicates temperature.

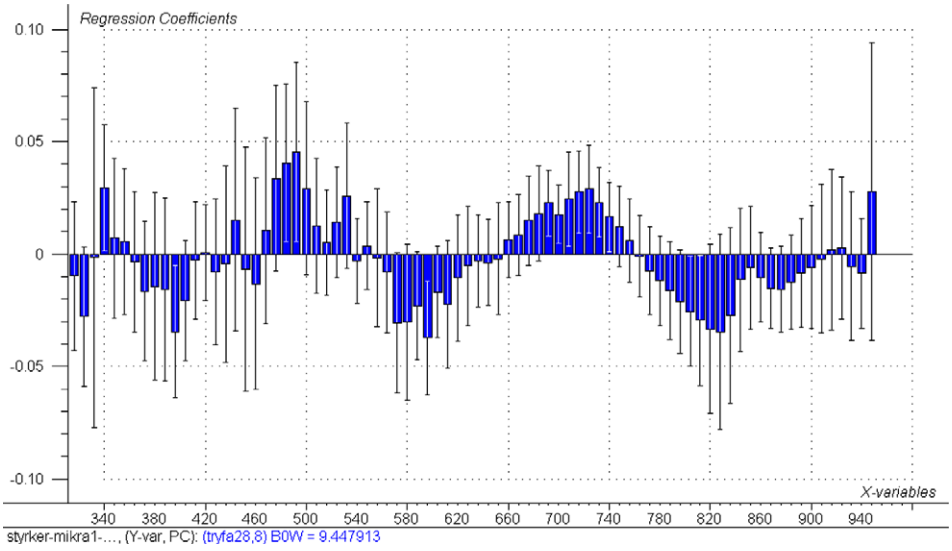

Fig. 16. Results from uncertainty testing on the regression coefficient, $\mathbf{b}_w$ (ordinate), for prediction of compressive strength at 28 days from the variables presented in Fig. 14 giving confidence intervals of 95%. Abscissa indicates temperature.

influences. The same dilemma about what variables to include in the modelling in the case of predicting compressive strength of fly ash cement from the microstructure of the cement could arise. Fig. 17 shows curves from DTGA of four fly ash cements containing about 20% fly ash, EN 197-1-CEM II/A-V 42.5 R. The curve indicates oxidation of perhaps ferrous mineral in the temperature range of approx. 370–550 °C and decarbonisation reaction in the temperature range of approx. 750–920 °C. The DTGA-curves will be difficult interpret quantitatively and accordingly defining variables to present the interpretation will be impossible. In any case the curves might contain some information valuable for giving a good model for prediction of compressive strength. Preliminary work on modelling of the compressive strength shows a high influence of loss on ignition of fly ash on the compressive strength at one day.

By application of sensitive analysis as described by Svinning [8] the influence of the microstructure could be examined more quantitatively. In [8] predictions of variation in compressive strength at 1 and 28 days from variation of latent variables of particle size distribution are shown. By including specific fineness as an additional variable a typical variation in the size distribution while the specific fineness is kept constant was simulated. The influence of a variable or a latent variable on a response variable, which could be a cement property, is significant if the confidence intervals of the predicted values do not overlap.

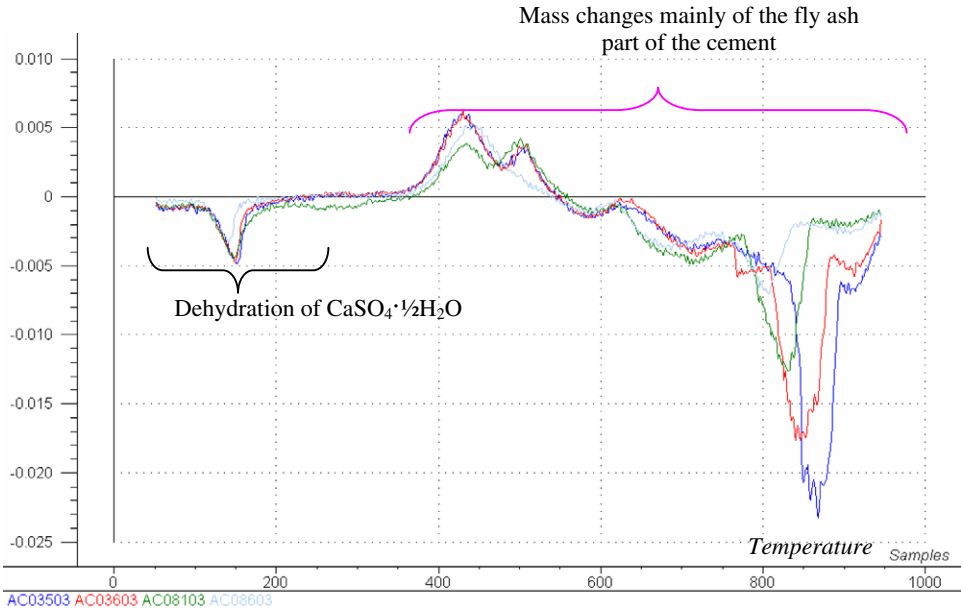

Fig. 17. DTGA of four samples of fly ash cement, EN 197-1-CEM II/A-V 42.5 R.

5. Conclusion

PLS of compressive strength up to 28 days on variables representing the characteristics of Portland cement gave maximum explained variance in compressive strength at 1, 2, 7 and 28 days of 93%, 90%, 79% and 67%, respectively. The high explained variance makes the prediction of the compressive strength up to 28 days from the characteristics reliable. Most of the variance in the compressive strength up to 28 days can be explained from the variances of the variables describing the mineralogy and the particle size distribution. The variables describing the superficial microstructure influenced the compressive strength at 28 days less than the compressive strength at one day.

The prediction ability makes it possible in this case to predict strength from cement characteristics and vice versa. Such a prediction can be utilized to design a cement to achieve target strength performance. By including the x-variables presenting the characteristic in the form of spectra no information will be lost and no further interpretation will be necessary to achieve a good prediction model. To achieve good strength prediction of fly ash containing cement, including the fly ash characteristics as spectra could be beneficial since the interpretation of these spectra is difficult.

The methodology demonstrated in the present paper is not limited to strength (which is easy measured directly), but it is also applicable to other more difficult/expensive achievable performance parameters that may beneficially be optimised via prediction from cement characteristics before actually documenting it for the most promising final products.

References

[1] Svinning K, Justnes H, Viggh E, Bremseth SK, Johansson S-E. Examination of clinkers from four Scandinavian Plants with respect to microstructure and cement properties. In: Proceedings of 22nd international conference on cement microscopy, Montreal; 2000. p. 137–153.
[2] Svinning K, Bremseth SK, Justnes H. X-ray diffraction studies on variations in microstructure of Portland clinker correlated with variations in production conditions in the kiln. World Cem 1996:80–6.
[3] Svinning K, Bremseth SK. The influence of microstructure of clinker and cement on setting time and strength development until 28 days. In: Proceedings of 18th international conference on cement microscopy, Houston; 1996. p. 514–513.
[4] Svinning K, Justnes H. Application of partial least square regression analysis in examination of correlations between production conditions, microstructure of clinker and cement properties, In: Proceedings of the 10th international congress on the chemistry of cement, Gothenburg; 1997. li038. p. 8.
[5] Goswani G, Mohapatra BN, Panda JD. Characterisation of burning condition by X-ray diffractometry. Cem Concr Res 1991;21:1176–9.
[6] Brüggemann H, Brentrup L. Correlations between mineralogical clinker parameters and cement strength. In: Proceedings of the 11th international conference on cement microscopy, Richmond; 1994. p. 226–245.
[7] Knöfel D. Interrelation between proportion of clinker phases and compressive strength of Portland cements. In: Proceedings of the 11th international conference on cement microscopy, New Orleans; p. 246–262.
[8] Svinning K. Chemom Intell Lab Syst 2006;84:177–87.
[9] Akkurt S, Tayfur G, Sever C. Fuzzy logic model for the prediction of cement compressive strength. Cem Concr Res 2004;34:1429–33.
[10] Tsivillis S, Parissakis G. A mathematical model for prediction of cement strength. Cem Concr Res 1988;28:9–14.
[11] Akkurt S, Ozdemir S, Tayfur G, Akyol B. The use of GA-ANN in the modelling of compressive strength of cement mortar. Cem Concr Res 2003;33:973–80.
[12] Martens H, Næs T. Multivariate calibration. 2nd ed. Chichester: Wiley; 1989.
[13] Martens H, Martens M. Food Qual Prefer 2000;11:5–16.
[14] Taylor HFW. Cement chemistry. 1st ed. London: Academic Press Ltd.; 1990. p. 24.